Acoustic Emission Source Location in Unidirectional Carbon-Fiber-Reinforced Plastic Plates with Virtually Trained Artificial Neural Networks

G. Caprino, V. Lopresto, C. Leone, I. Papa

Department of Materials and Production Engineering, University of Naples "Federico II," Piazzale Tecchio, 80, Naples 80125, Italy

Received 28 April 2011; accepted 28 April 2011
DOI 10.1002/app.34758
Published online 9 August 2011 in Wiley Online Library (wileyonlinelibrary.com).

ABSTRACT: Acoustic emission (AE) source location in a unidirectional carbon-fiber-reinforced plastic plate was attempted with artificial neural network (ANN) technology. The AE events were produced by a lead break, and the response wave was received by piezoelectric sensors. The time of arrival, determined through the conventional threshold-crossing technique, was used to measure the dependence of the wave velocity on the fiber orientation. A simple empirical formula, relying on classical lamination and suggested by wave-propagation theory, was able to accurately model the experimental trend. On the basis of the formula, virtual training and testing data sets were generated for the case of a plate monitored by three transducers and were adopted to select two potentially effective ANN architectures. For final validation, experimental tests were carried out, with the source positioned at predetermined points evenly distributed within the plate area. A very satisfactory correlation was found between the actual source locations and those predicted by the virtually trained ANNs. © 2011 Wiley Periodicals, Inc. J Appl Polym Sci 122: 3506–3513, 2011

Key words: fibers; plastics; composites; damage zone

INTRODUCTION

Acoustic emission (AE) has long been recognized as a viable technique for the real-time monitoring of metallic and composite structures, giving useful information not only on the presence of defects but also on their criticality.[1–4] In the case of composites characterized by a multiplicity of failure modes, the possibility has also been devised to discriminate among the different damage mechanisms by a careful analysis of the wave features.[5,6] Therefore, AE methods are promising monitoring systems, helpful in improving safety and reducing maintenance costs in industrial applications.

An attractive feature of AE is its ability to locate defects. Tobias[7] showed that for isotropic plates, the problem of source location could be solved in a closed form by triangulation if the difference in the arrival times of the acoustic waves at three probes placed on the plate surface is known. Although this solution seems to be straightforward, many drawbacks, essentially correlated with the laws governing wave propagation, arise where practical applications are concerned.

An acoustic wave generated by a localized source in a platelike structure propagates in two basic modes: the symmetric (also known as the extensional) mode, associated with the in-plane properties of the plate, and the antisymmetric (flexural) mode, which depends on the flexural properties. Both these modes are dispersive, that is, their velocity is a function of the frequency. Thus, the pulse changes shape with increasing distance from the source. This phenomenon greatly affects the precision in source location with the threshold-crossing technique because the individuation of the phase point of the waveforms to assume as a reference for time measurement is not easy.[8,9]

The dispersive nature of extensional waves clearly appears only at quite high frequencies. For sufficiently low frequencies, the symmetric waves are substantially nondispersive, and their velocity can be calculated by very simple analytical tools.[8,10] These attributes have been exploited in commercial AE instrumentation to suitably improve source location.

Although strongly dispersive at low frequencies, flexural waves offer an outstanding advantage compared with extensional ones: their magnitude is much larger, so they propagate greater distances; this allows the monitoring of large structures with the use of a limited number of sensors. This potentiality explains the great deal of work devoted to the propagation of acoustic waves in dispersive media and to methods for reliable measurement of the time of arrival (TOA) under these conditions.[6–8,10,11]

Correspondence to: V. Lopresto (lopresto@unina.it).

Because of the anisotropy of composite laminates, AE source location in these materials encounters additional difficulties. In fact, because of the dependence of the elastic properties on direction, the wave velocity (v_e) is also a function of orientation; this renders useless the closed-form formulation proposed by Tobias.[7] Consequently, triangulation is performed by iteration.[11] Alternatively, another technique, based on the minimization of an error function suitably defined, was recently proposed.[12]

Notably, the location methods available nowadays imply the knowledge of the laminate elastic properties. Therefore, the error in location is influenced not only by the TOA precision but also by the ability to accurately calculate the engineering in-plane and flexural elastic moduli and the shear moduli along the thickness direction. This is not always simple to predict because of the laminar structure of the composites of technical interest.[13] An approach potentially useful for overcoming this difficulty is offered by artificial neural networks (ANNs), which have found widespread application in many scientific domains, providing reliable solutions.[14,15] ANN analysis is a general method of nonlinear regression, applicable in principle wherever some input variables determine output results following rules not amenable to a mathematical formulation. ANNs can learn by examples arranged according to a training set, so in the case of AE source location, the role played by the elastic moduli is intrinsically taken into account in the training data.

SCOPE

The engineering problem faced in this study is schematically depicted in Figure 1. A square composite plate is monitored by three AE sensors (P_i's), located as shown in the figure. When an acoustic signal is generated at point *S*, the wave travels within the material, achieving the probes after times depending on both the length (d_i) and the orientation of the lines connecting the source point to each sensor. Knowing the TOA at each sensor, the source location (i.e., the coordinates *x* and *y* of point *S*) was determined with ANN.

If a model able to yield TOA as a function of the fiber orientation (θ) and distance from the source is available, the TOA at each probe in Figure 1 can be easily calculated. Therefore, the training set necessary for network learning can be developed without experimental tests. In principle, this offers an attractive means to virtually train the candidate ANN architectures and to find the most effective solution.

The previous considerations illustrate the significance of this work, where a simple empirical law, useful for providing TOA in an orthotropic composite plate, was assessed by experimental tests. Using this law, we constructed a virtual training set and used it to design two potentially efficient ANNs. The precision of the networks was estimated by comparison of the ANN predictions with the results of appropriate AE tests.

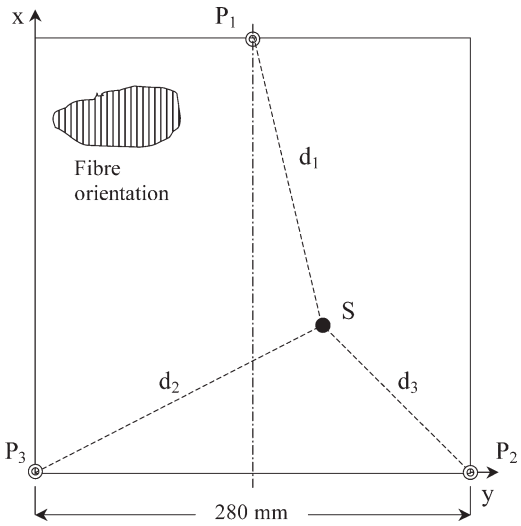

Figure 1 Square composite plate monitored by three AE sensors (P_1, P_2, P_3).

The characteristics of the AE signals were not affected by stacking sequence of the laminate but were dependent on the failure mechanism or source.[16,17] Because the difficulty in source location increased with increasing anisotropy ratio of the material under concern,[11,18] a unidirectional carbon-fiber-reinforced plastic (CFRP), characterized by a very high anisotropy ratio, was purposely selected in this work. However, in the literature, many researchers[16–19] have demonstrated the consistency in AE parameters for different classes of laminates, proving the efficiency of ANN in characterizing them. In particular, Bar et al.[16] successfully found identical characteristics of AE events between unidirectional composites and laminates different in stacking sequences and the classification of AE parameters through ANN.

EXPERIMENTAL

A square unidirectional CFRP laminate, 340 mm on a side and 2 mm in nominal thickness (*t*) was fabricated by the manual laying up of eight layers of BMS 8-276 Toray prepreg, which were vacuum-bagged and cured under a press at 177°C temperature and 0.5 MPa pressure. The laminate was trimmed by a diamond cutting tool to obtain a square panel 300 mm on a side, which was used in the subsequent experimental campaign.

The source in all AE tests was a lead break (Pentel 2H, 0.5 mm). The waves were detected by a Vallen AMSY4 16-channel instrument (Vallen-Systeme Gmbh, Ichking, Munich, Germany), with VS150-M

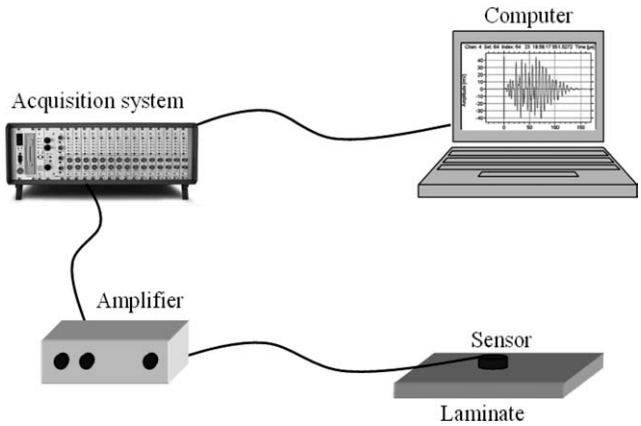

Figure 2 AE measuring chain.

transducers resonant at 150 kHz, 20.5 mm in diameter, and coupled to the plate by vacuum grease. The signals were filtered by 95-kHz high-pass filters, amplified by 34 dB with acoustic emission preamplifiers (AEP3), and then transferred to an acoustic signal preprocessor (ASIPP) board for digitalization and extraction of the relevant AE parameters. The acquisition time was 0.2 μs, whereas the threshold for TOA measurement was fixed at 28.8 dB. All of the data were stored in a computer for subsequent visualization and analysis.

A scheme of the acquisition chain is depicted in Figure 2.

The ANN architectures were designed by Peltarion Synapse commercial software, run on a MacBook computer equipped with a 2.16-GHz Intel Core 2 Duo processor in Windows ambient.

RESULTS AND DISCUSSION

In this section, the possibility of predicting TOA as a function of distance from the source and material orientation is first presented and discussed. Then, the optimization of the ANN architecture is addressed. Finally, the experimental validation of the ANN performances is demonstrated.

TOA prediction

As noted previously, the dispersive nature of acoustic waves can result in an incorrect evaluation of TOA through the threshold-crossing technique. Of course, because TOA was selected in this work for source location, the possibility of succeeding in accomplishing the goal was critically dependent on the ability to accurately measure this parameter.

To verify the consistency of the TOA values provided by the AE system, acoustic waves were excited by lead breaks and detected by three sensors, located at known distances from the source along a straight line (Fig. 3) oriented at θ with respect to the fiber direction. The distance of the source from the center of first sensor (S_1) was approximately 20 mm, and the distance between the two subsequent sensors (S_2, S_3) was 100 mm. Although, in theory, the material behavior should be the same for $+\theta$ and $-\theta$, we preferred to scan the entire range from -90 to 90°. In fact, deviations of the actual acoustic response from what is expected on the basis of material symmetry, which probably reflect imperfections in the composite structure, have been noticed sometimes.[12]

The amplitude of the signal measured by the AE instrumentation in correspondence of S_1 was typically 96–100 dB, regardless of the angle (θ) considered. Of course, because of attenuation, the signal amplitude decreased steadily with increasing traveling distance. However, the amplitude was in the range 67–77 dB, well beyond the threshold value set (28.8 dB) at the sensor (S_3) farthest from the source.

Typical plots of the acoustic signals recorded at each sensor are shown in Figure 4. In each of the diagrams in the figure, $t = 0$ conventionally coincides with the time where the threshold amplitude was overcome at the specific sensor, whereas the actual time (in μs) is visible on the upper right corner.

From the differences in TOA (Δt's) between two subsequent probes, two independent values of v_e were defined as follows:

$$v_e = \frac{\Delta d}{\Delta t} \tag{1}$$

where Δd is the distance between the transducers and was calculated for each experimental test.

In Figure 5, the experimental v_e values are plotted versus θ. In the figure, different symbols are used to distinguish between the velocities measured within the intervals S_1–S_2 (▲) and S_2–S_3 (○), respectively.

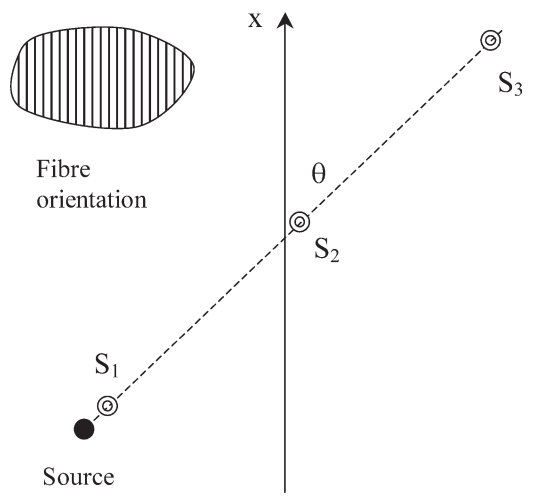

Figure 3 Experimental setup for the measurement of TOA.

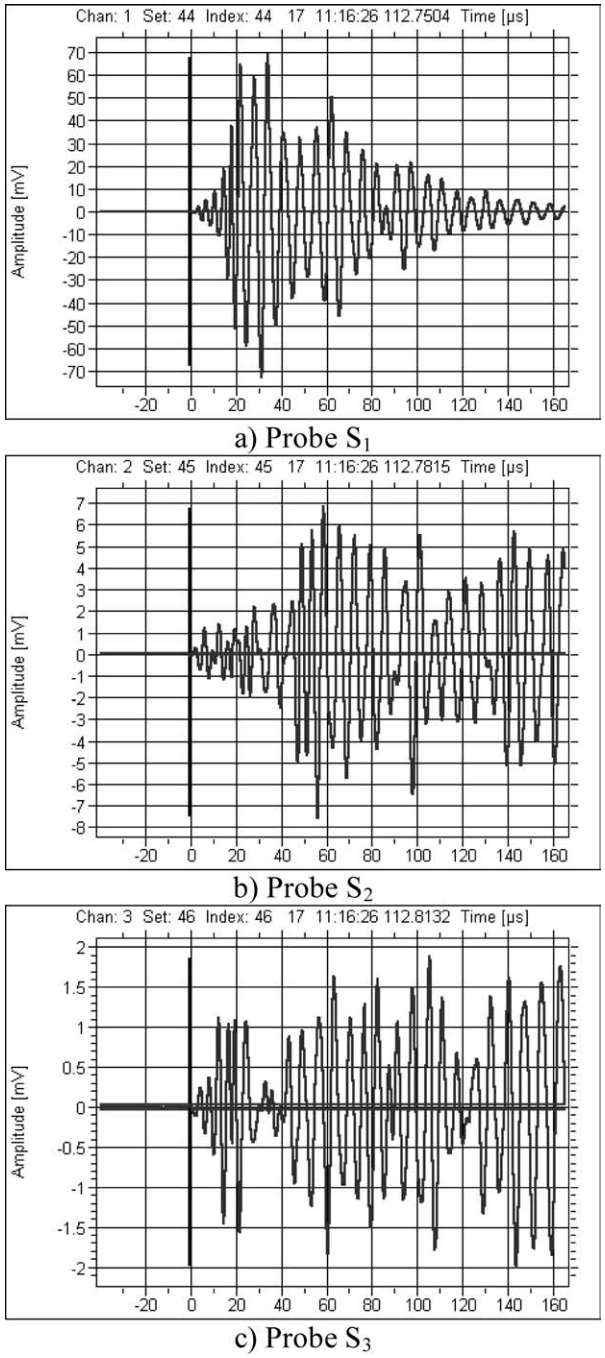

Figure 4 Waveforms recorded by the three probes ($\theta = 45°$).

As anticipated from the material anisotropy, v_e was strongly dependent on orientation, steadily decreasing with increasing θ. The symmetry of v_e with respect to $\theta = 0°$ was substantially fulfilled, with the largest difference (ca. 11%) occurring between $+15$ and $-15°$. In general, the scatter in the data was low. Besides, v_e was independent of distance when we assessed the consistency of the TOA measurements; therefore, if a suitable expression able to yield $v_e = v_e(\theta)$ is available, Eq. (1) can be used to theoretically predict TOA for whichever orientation and distance from the source.

The continuous line in Figure 5 is the graphical expression of the following equation:

$$v_e = \sqrt{\frac{E_x}{\rho(1 - \nu_{xy}\nu_{yx})}} \tag{2}$$

where E is Young's modulus and ν is Poisson's ratio and the indices x and y affecting them designate the propagation direction and its perpendicular, respectively. Also, ρ is the material density. Equation (2) was suggested by the following well-known relationship:[8]

$$v_e = \sqrt{\frac{E}{\rho(1 - \nu^2)}} \tag{3}$$

This equation is valid for extensional waves propagating in an isotropic medium, with the quantity $E/(1 - \nu^2)$ substituted with its equivalent for an orthotropic material: $E_x/(1 - \nu_{xy}\nu_{yx})$.

To draw the curve in Figure 5, attempt values were assigned to the basic elastic moduli of the lamina, E_1, E_2, G_{12}, and ν_{12}, where G_{12} is the shear modulus; then, the material moduli in Eq. (2) were calculated by classical lamination theory; finally, the basic moduli were varied until a satisfactory correlation of the curve with the experimental trend was found. ρ was assumed to be 1.55 g/cm^3, typical of BMS 8-276. The results in Figure 5 were obtained with the following values: $E_1 = 142$ GPa, $E_2 = 9.2$ GPa, $G_{12} = 6.7$ GPa, and $\nu_{12} = 0.34$.

Indeed, the correlation between the experimental points in Figure 5 and Eq. (2) is outstanding. Therefore, a simple formula is available for the accurate prediction of TOA. As is shown later, having this tool can significantly ease the development of the ANNs devoted to source location.

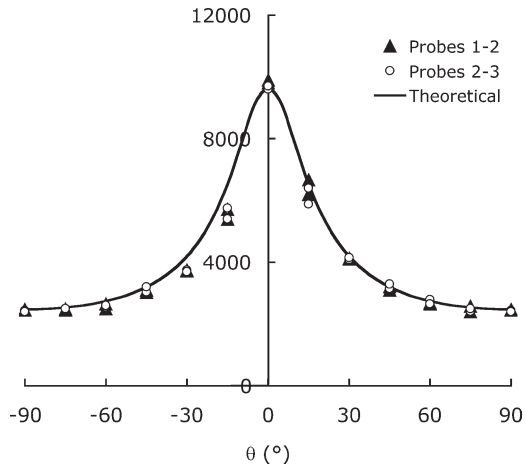

Figure 5 v_e against θ. Different symbols are used to distinguish between the velocities measured within the intervals S_1–S_2 (▲) and S_2–S_3 (○), respectively.

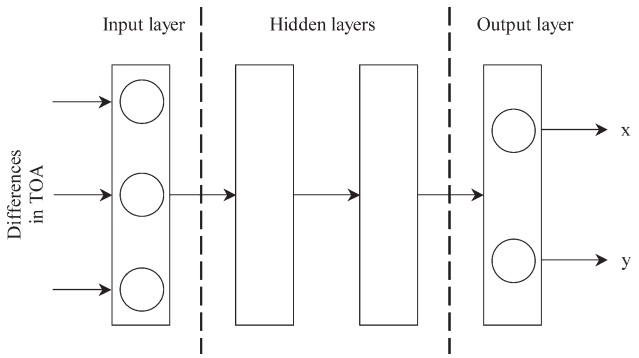

Figure 6 General structure of the ANNs examined.

ANN architecture

In an ANN, simple processing elements (the neurons) are connected together to form a complex network of nodes. Some of the neurons are destined to receive the input parameters and form the input layer; others provide the desired numerical values and are collected in the output layer. Between the input and output layers, one or more hidden layers are contained, each holding an assigned number of neurons. In flowing along a connection, the signal is multiplied by a specific value (weight), which determines its effect on the output.

When an ANN has been designed, its ability to solve an engineering problem must be exploited in a learning stage. To do this, a training data set, consisting of input values and corresponding desired output values, must be available and must be analyzed by the network. The learning mechanism consists of an iterative process, during which a progressive change of the weights affecting each connection occurs, according to a preset law (transfer function), until a satisfactory agreement between the desired and predicted outputs is achieved.

The consistency in AE parameters of the signals generated in composite laminates proves the efficiency of ANN, and the possible diagnosis of the actual damage performed instantly with a well-developed ANN is demonstrated.[16,17,19] One of the most challenging tasks in designing an ANN network is its optimization, for which no definite rules exist at present. The problem is complicated by the large number of possible choices, which involve the network architecture (e.g., number of layers, nodes in each of them, number of connections between the nodes), transfer function typology, number of training cycles (epochs), sensors placement, and so on.[18]

To limit the ANN design work, preliminary constraints were assumed in this study. The differences in TOA recorded by the three probes (P_i's) in Figure 1 were adopted as input parameters, so the input layer was made of three neurons, and the output layer was supplied with two nodes, providing the abscissa and the ordinate of the source S.

From theory, there is no reason to use neural networks with more than two hidden layers, by which whichever function can be represented with accuracy.[14] Therefore, in the determination of a satisfactory ANN architecture, the number of hidden layers (N_{hl}) was held constant ($N_{hl} = 2$), and the number of their nodes was varied. In all, 15 different ANN architectures were analyzed. In each of them, the number of nodes in the hidden layers was randomly determined; this fulfilled the condition of a total number of nodes comprised in the range 6–30.

The general structure of the ANNs examined (Fig. 6) pertained to multilayer perception and was trained according to the backpropagation algorithm. Other relevant parameters, collected in Table I, were set to their default values and were not altered along all of the ANN design stage.

As stated previously, to proceed to the learning stage of an ANN, a training set is required. The usual way to build the training set is to perform a sufficient number of experimental tests with suitable variation of the location of the source S (Fig. 1) and to measure the associated TOA. This route is time-consuming because hundreds of data are needed to be confident in a satisfactory accuracy of the network. However, if the dependence of v_e on the orientation is given, from it, the TOA can be simply calculated, knowing the source location. This method was applied in this work: 2500 different location points were selected by a random-number generator; for each, the TOA at the three sensors was theoretically evaluated as the ratio d_i/v_e (Fig. 1), with Eq. (1) used to calculate v_e; finally, 15% of the location points theoretically evaluated were used for cross-validation during the training stage. Training was stopped after a maximum of 5×10^4 iterations or when the error signaled by the learning curve dropped below 0.005%, whichever of these conditions was met first.

After training, the ANNs examined were subjected to a validation test to assess their effectiveness. A testing set, consisting of 14 unknown location points, was built according to the same procedure described for the training set and was presented to the network. The distance (D) between each input and

TABLE I
Relevant Parameters Adopted in the Development of the ANNs

Stage	Feature	Value
Design	Forward rule	No rule
	Back rule	Step rule
	Transfer function	Tanh sigmoid
	Step	0.1
	Momentum	0.7
Training	Batch length	1
	Validation interval	5

TABLE II
Accuracy Parameters Characterizing the ANNs Considered in this Study

Data source	ANN architecture	D_m (mm)	SD (mm)	D_c (mm)	D_{max} (mm)
Testing set	3/10/8/2	1.24	0.76	2.00	2.62
	2/10/8/2	0.94	0.37	1.30	1.58
Experimental	3/10/8/2	2.18	1.99	4.17	6.95
	2/10/8/2	1.85	2.04	3.89	7.03

associated predicted point was calculated, and the characteristic distance (D_c) was arbitrarily defined as follows:

$$D_c = D_m + SD \quad (4)$$

where D_m is the arithmetic mean of the distance and SD is the standard deviation and was assumed as an error parameter, on the basis of which the different ANN architectures were ranked.

The best ANN network, selected according to the previous procedure, consisted of a 3/10/8/2 structure; that is, it was made of 10 and 8 nodes in the first and second hidden layers, respectively, and had three nodes in the input layer and two nodes in the output layer. For this solution, $D_c = 2.0$ mm, with $D_m = 1.24$ mm and SD = 0.76 mm, computed (Table II) after about 4×10^4 epochs, requiring a training time of approximately 16 min, was accomplished.

A comparison of the points included in the testing set and their positions as predicted by the 3/10/8/2 ANN is shown in Figure 7, where the network is individuated by the label 3IN (three input nodes). The black arrow in the figure indicates the point in correspondence of which the maximum distance ($D_{max} = 2.62$ mm) of the predicted from the real source location was found.

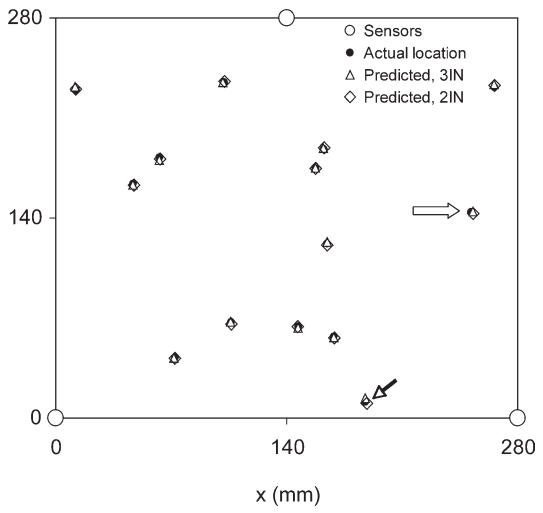

Figure 7 Comparison between the source locations included in the testing set and those predicted by ANNs.

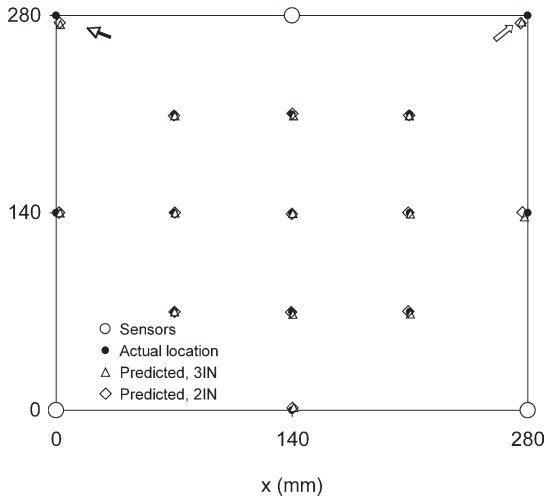

Figure 8 Comparison between the experimental and predicted source locations.

Indeed, only two of the three differences in TOA used as input data for the ANN architectures in Figure 6 are independent because a simple relationship correlating them could be easily established. To verify the effect of the redundant input parameter on the ANN performances, a 2/10/8/2 network, identical to the 3/10/8/2 except in the number of input nodes, was designed and trained. Approximately 4.5 $\times 10^4$ training iterations, completed in 19 min, were required to achieve the assigned accuracy. The white diamonds in Figure 7 are the predictions of this ANN (labeled as 2IN for two input nodes), fed with the appropriate differences in TOA included in the testing set. The white arrow indicates the location point where the maximum error ($D_{max} = 1.58$ mm) was verified. The main accuracy parameters are shown in Table II. From them, the 2/10/8/2 network was foreseen to perform better than its 3/10/8/2 counterpart. Therefore, it seemed that the redundant input parameter did not result in a more effective response of ANN. Furthermore, this finding suggests that an even more efficient solution might be individuated by an accurate optimization procedure.

Experimental validation

To assess the two ANN architectures selected, experimental tests were performed with, as source locations, the points represented by the black circles in Figure 8. Acoustic waves were generated by lead breaks, and the measured TOAs were given in input to the trained ANNs, which provided the predicted locations (open symbols in the figure).

The correlation between the actual and predicted source locations was very satisfactory. Besides, the 2/10/8/2 configuration seemed to be more effective than the 3/10/8/2 one (Table II), although its

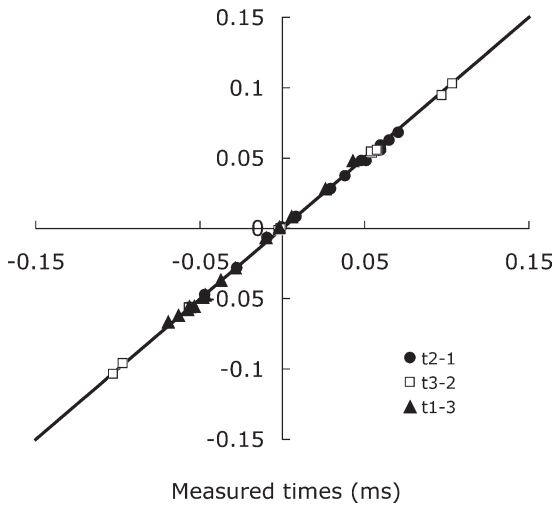

Figure 9 Comparison of the theoretical and experimental differences in the TOAs of the source waves at the three AE sensors.

superiority was less evident than expected from the virtual testing results.

All the D_m, SD, D_c, and $D_{\max}$ values derived from the experimental tests were higher than their counterparts obtained in the testing stage. This phenomenon was anticipated and reflected the scatter in the experimental data that was absent in the testing set.

With theory, the differences in TOAs between the sensors (P_i's) in Figure 1 were calculated and compared with the experimental ones. The results are shown in Figure 9, where the label t_{i-j} designates the difference in TOAs between probes i and j.

From Figure 9, the agreement between theory and experiments was excellent, as witnessed by the symbols, sensibly falling along the 45° continuous straight line, which was drawn for reference. This explains why the virtual ANN training was successful in yielding an effective architecture, which was directly usable for interpreting the experimental results.

Additional considerations

From our results, we found that a virtually trained ANN was able to correctly locate AE sources in orthotropic laminates. To achieve this task, two tools were necessary: (1) an experimental technique that provided a precise measurement of the TOA under the operating conditions and (2) a reliable method, empirically assessed or theoretically developed, through which the TOA associated with a generic point within the area monitored could be estimated.

The accuracy of the predictive method determined the correctness of ANN training. It is important to realize that, whereas Eq. (2) was used in this work to express $v_e = v_e(\theta)$, whichever function was able to follow the experimental trend in Figure 5 (e.g., a polynomial of suitable degree) would have been equally useful to the aim in the case examined. It was inferred that possible differences between $v_e(\theta)$ and $v_e(-\theta)$ resulting from imperfections in the material structure could be accounted for by selection of the most appropriate relationship.

The precision in the measurement of TOA directly influenced the goodness of the ANN input data. In the case examined, similarly to the findings of other researchers,[7,12] the threshold-crossing technique was adequate for yielding consistent values of TOA. However, alternative methods, among which the most popular was the Gabor wavelet transform, have been also presented and have been demonstrated to be able to provide reliable TOA estimates when the dispersive nature of the waves renders the task more difficult.[5,10,11]

It is important to note that the ability of a trained ANN to solve location problems is strictly dependent on the sensor positions. Changing the probes' arrangement will require a new training stage and perhaps a different network architecture for a satisfactory response. On one hand, this is a limitation intrinsic to the method; on the other hand, the results obtained in this work suggest a virtual means for studying the effect of different parameters (e.g., sensors location, number of sensors employed in monitoring) on the expected accuracy of the predictions.

In this case, where a flat panel 780 cm^2 in area was monitored by three AE sensors, the maximum error in the source location was about 7 mm (Table II). A comparison of this result with equivalent predictions based on other location algorithms to judge the effectiveness of the method proposed was not straightforward. Indeed, many factors, among them the sensor number and location, extent of monitored area, and material anisotropy, play a major role in affecting the precision. However, a situation similar to that faced here was experienced by Jeong and Jang,[11] who used a unidirectional graphite/epoxy square plate 600 mm on a side to monitor the area within three sensors arranged according to a triangular array. The distance between the probes was not specified by the authors; however, from the figures available, the area under control was comparable to the one considered here. The maximum error in location, determined by classical triangulation, was 6.3 mm. A slightly better precision was achieved when the laminate monitored was quasi-isotropic. The maximum error was quoted to be 12.4 mm by Banerjee et al.,[20] who used nine piezoelectric sensors evenly distributed over a 400-cm^2 area of a stiffened CFRP panel, together with a sophisticated analysis based on high-frequency wave propagation data and low-frequency vibration measurements. Far less accurate estimates were documented by Coverley and Staszewski,[18] who embedded 12 SMART

sensors in a 608 × 304 mm^2 quasi-isotropic composite panel, trying to predict the impact location by a triangulation technique coupled with an optimization genetic algorithm procedure. When only three of the sensors were used to predict the impact location, errors on the order of many centimeters were discovered for both of the point coordinates.

The application of ANNs in source location appears promising not only for flat but also for curved composite components. Prevoroski et al.[21] monitored [+55/−55] glass fiber–epoxy filament wound tubes by six AE transducers distributed over a 500-cm^2 area. The TOA data were sent to an ANN for source location; this resulted in an error lower than 8 mm.

CONCLUSIONS

In this work, the AE source location in a unidirectional CFRP plate was predicted by virtually trained ANNs with the differences in TOAs of the waves between three sensors places on the material surface. From the results obtained and discussed, the main conclusions are as follows:

- If a reliable method is available to correlate the TOA with the orientation and distance of a generic point from the source, a satisfactory ANN architecture can be found and exploited without need of experimental tests.
- The virtually trained ANNs were able to locate the source with satisfactory accuracy; for the best solution found, D_m of the predicted from actual point location was 1.85 mm, SD was 3.89 mm, and D_{max} was 7.03 mm.
- The possibility of using ANN in the performance of virtual testing to study the effect of sensor number and arrangement on the accuracy of the measurements was supported by the results obtained.

References

1. Drouillard, T. F. J Acoust Emiss 1996, 14, 1.
2. Nondestructive Testing Handbook, 3rd ed.; Acoustic Emission Testing: Columbus, OH, 2005; Vol. 6.
3. Caprino, G.; Teti, R.; De Iorio, I. Compos B 2005, 36, 365.
4. Philippidis, T. P.; Assimakopoulou, T. T. Compos Sci Technol 2008, 68, 840.
5. Mal, A. Int J Solids Struct 2002, 39, 5481.
6. Marec, A.; Tomas, J.-H.; El Guerjouma, R. Mech Syst Sign Pr 2008, 22, 1441.
7. Tobias, A. Non-Destruct Test 1976, 9, 9.
8. Ziola, S. M.; Gorman, M. R. J Acoust Soc Am 1991, 90, 2551.
9. Kinsler, L. E.; Frey, A. R.; Coppens, A. B.; Sanders, J. V. Fundamentals of Acoustics; Wiley: New York, 2000.
10. Wang, L.; Yuan, F. G. Compos Sci Technol 2007, 67, 1370.
11. Jeong, H.; Jang, Y.-S. Compos Struct 2000, 49, 443.
12. Kundu, T.; Das, S.; Martin, S. A.; Jata, K. V. Ultrasonics 2008, 48, 193.
13. Reddy, J. N.; Wang, C. M. Compos Sci Technol 2000, 60, 2327.
14. Ripley, B. D. Pattern Recognition and Neural Networks, Cambridge University Press: Cambridge, England, 1996.
15. Bhadeshia, H. K. D. H. ISIJ Int 1999, 39, 966.
16. Bar, H. N.; Bhat, M. R.; Murthy, C. R. L. Compos Struct 2004, 65, 231.
17. Giordano, M.; Calabro, A.; Esposito, C.; D'Amore, A.; Nicolais, L. Compos Sci Technol 1998, 58, 1923.
18. Coverley, P. T.; Staszewski, W. J. Smart Mater Struct 2003, 12, 795.
19. Su, Z.; Ye, L. Compos Struct 2004, 66, 627.
20. Banerjee, S.; Ricci, F.; Monaco, E.; Mal, A. J Sound Vibrat 2009, 322, 167.
21. Prevoroski, Z.; Landa, M.; Blahacek, M.; Varchon, D.; Rousseau, J.; Ferry, L.; Perreux, D. Ultrasonics 1998, 36, 531.